Polymer Chemistry

PAPER

View Article Online
View Journal | View Issue

Cite this: *Polym. Chem.*, 2015, **6**, 2531

Bis(2-oxoindolin-3-ylidene)-benzodifuran-dione-based D–A polymers for high-performance n-channel transistors†

Guobing Zhang,*[a,b] Jinghua Guo,[a,c] Min Zhu,[a,c] Peng Li,[a,c] Hongbo Lu,[a,b] Kilwon Cho[d] and Longzhen Qiu*[a,b]

Conjugated polymers based on a bis(2-oxoindolin-3-ylidene)-benzodifuran-dione (BIBDF) unit displayed promising performances for their application in organic thin-film transistors (OTFTs). Herein, three new BIBDF-based donor–acceptor (D–A) polymers, containing thieno[3,2-*b*]thiophene (TT), (*E*)-2-(2-(thiophen-2-yl)vinyl)thiophene (TVT) and (2-(thiophene-2-yl)alkynyl)thiophene (TAT) as donors, were synthesized and characterized. The results indicated that the donor unit plays important roles in affecting the absorption bands, HOMO levels, lamellar packing and π–π stacking distances of the BIBDF-based polymers. The OTFT devices based on the three polymers were fabricated, and their field-effect performance and environmental stability were also characterized. All three BIBDF based polymers showed good n-type field-effect characteristics. The **PBIBDF-TT** showed the highest electron mobility of 0.65 $cm^2 V^{-1} s^{-1}$ and the best environmental stability, while the **PBIBDF-TAT** showed the lowest electron mobility of 0.13 $cm^2 V^{-1} s^{-1}$. The corresponding crystalline structures and morphologies revealed that the **PBIBDF-TT** and **PBIBDF-TVT** showed close π–π distances and long-range ordered, lamellar crystalline structures both of which contributed to the high charge carrier mobility. The **PBIBDF-TAT** with close π–π distances but poor crystalline structures showed miserable performance. Overall, this work showed the correlation of the microstructures and properties of BIBDF-based polymers, and the field-effect performances can be effectively optimized by introducing different donor units.

Received 5th December 2014,
Accepted 29th January 2015

DOI: 10.1039/c4py01683a

www.rsc.org/polymers

1. Introduction

Solution-processable conjugated polymers have attracted considerable attention due to their application in low-cost, lightweight and flexible organic thin-film transistors (OTFTs).[1] Among conjugated polymers, donor–acceptor (D–A) polymers have been extensively studied because their molecular designs allow one to tailor their electronic structures, including the photon absorption, highest occupied molecular orbital (HOMO) energy levels, lowest unoccupied molecular orbital (LUMO) energy levels and energy bandgaps.[2] Benefiting from the development of new D–A conjugated polymers, as well as optimized processing and device fabrication, great progress has been made in developing high-performance polymer semiconductors. Excellent hole transporting polymer semiconductors with mobility comparable to small molecules have been developed in the past few years.[3] However, the overall development of n-channel polymers still lags behind their p-channel counterparts in terms of amount, mobility, and so on.[4] To design and synthesize an n-channel polymer, the LUMO energy level is the key factor and must be lower than or close to −4.0 eV for stable electron transport.[5] For a D–A conjugated polymer, the incorporation of a strong electron-deficient acceptor unit into a D–A polymer can usually give rise to a low-lying LUMO (high electron affinity) level which has been confirmed to be beneficial for the stability of charge transport.[6] Therefore an important approach in developing n-channel polymer semiconductors is the synthesis of a D–A polymer, which by virtue of its modular nature can facilitate the tuning of the LUMO energy level (~−4.0 eV) depending on the choice of the strong electron-accepting unit.

[a]*Key Lab of Special Display Technology, Ministry of Education, National Engineering Lab of Special Display Technology, State Key Lab of Advanced Display Technology, Academy of Opto-Electronic Technology, Hefei University of Technology, Hefei, 230009, China. E-mail: gbzhang@hfut.edu.cn, lzqiu@ustc.edu*
[b]*Key Laboratory of Advanced Functional Materials and Devices, Anhui Province, Hefei, 230009, China*
[c]*Department of Polymer Science and Engineering, School of Chemistry and Chemical Engineering, Hefei University of Technology, Hefei, 230009, China*
[d]*Department of Chemical Engineering, Pohang University of Science and Technology, Pohang, 790-784, Korea*
†Electronic supplementary information (ESI) available. See DOI: 10.1039/c4py01683a

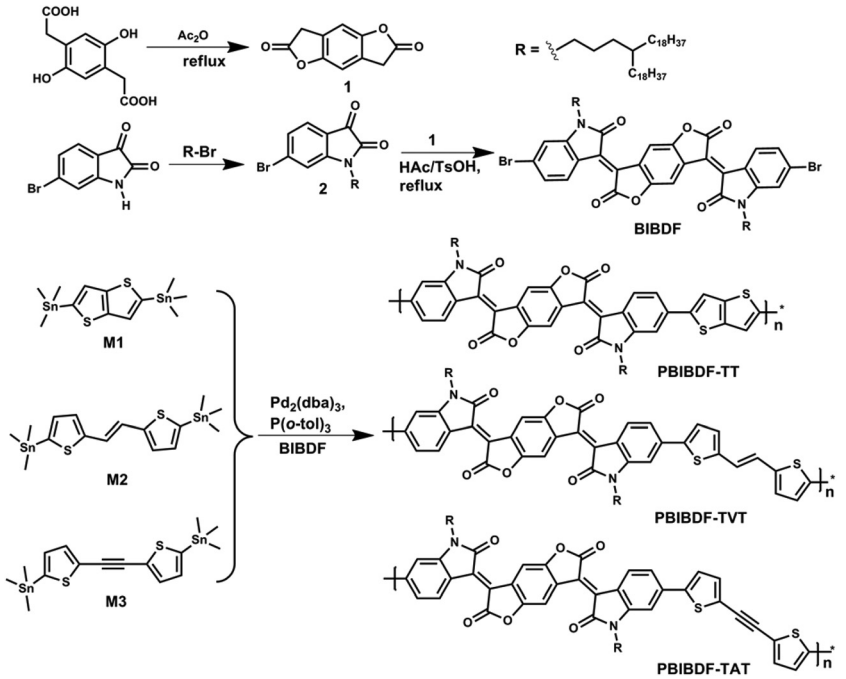

Scheme 1 The synthetic route to monomer and polymers.

So far, the D–A polymers found to be typical n-channel semiconductors for developing high-performance OTFTs have only focused on those containing lactam- or imide-based acceptor units such as diketopyrrolopyrrole (DPP), naphthalene diimide (NDI) and perylene diimide (PDI).[7] Recently, a new electron-deficient fused aromatic ring bis(2-oxoindolin-3-ylidene)-benzodifuran-dione (BIBDF) and its polymers have been developed by us and other groups.[8] BIBDF has a large fused aromatic ring with symmetric and planar structure, which should increase the π–π overlap and intramolecular interaction. The two lactone groups in the central core coupled with the two lactam groups make the BIBDF unit strongly electron deficient.[8d] Indeed, the reported polymers based on a BIBDF unit exhibited n-type or ambipolar transport characteristics with remarkably high mobilities approaching 1 $cm^2\ V^{-1}\ s^{-1}$.[8a–c] Although a few polymers based on BIBDF have been reported and high electron mobilities have been achieved, the BIBDF based n-type materials are still worth further investigation considering their promising performances.

In this paper, we presented the synthesis of three new D–A polymers (Scheme 1) based on a BIBDF unit and different electron-donors (thieno[3,2-*b*]thiophene (TT), (*E*)-2-(2-(thiophen-2-yl)vinyl)thiophene (TVT) and (2-(thiophene-2-yl)alkynyl)thiophene (TAT)), and the characterization of their thermal, optical, electrochemical, microstructural, and OTFT properties. The results indicated that the BIBDF-based polymers showed varied absorption bands and molecular energy levels and also different micro-structures in solid films; thus, three polymers display varied field-effect performances in OTFT devices. This work has showed the correlation of the microstructures and properties of BIBDF-based polymers, and the field-effect performances can be effectively optimized by introducing different donor units.

2. Results and discussion

2.1. Synthesis and characterization

The synthetic routes of the relevant monomers and polymers are illustrated in Scheme 1. The compound benzo[1,2-*b*:4,5-*b*′]-difuran-2,6(3*H*,7*H*)-dione (**1**) was conveniently synthesized from the dehydration reaction of 2,5-dihydroxy-1,4-benzenediacetic acid. 6-Bromoindoline-2,3-dione was *N*-alkylated with a 4-bromo-alkyl group to form 6-bromo-1-(4-octadecyldocosyl)-indoline-2,3-dione (**2**), which was easily converted to the dibromo-monomer **BIBDF** by reacting with compound **1** in acetic acid at about reflux temperature. In order to obtain good solubility for the final BIBDF-based polymer, two long branched 4-octadecyldocosyl chains were introduced into a **BIBDF** unit. Finally, three polymers were synthesized by Stille cross-coupling polymerizations with a 1 : 1 monomer ratio in the presence of tris(dibenzylidene-acetone)dipalladium-($Pd_2(dba)_3$) as a catalyst and tri(*o*-tolyl)phosphine ($P(o\text{-tol})_3$) as a ligand to give a black solid. **PBIBDF-TT** and **PBIBDF-TVT** displayed good solubility in solvents such as tetrahydrofuran, chloroform and chlorobenzene at room temperature. **PBIBDF-TAT** was only soluble in hot chloroform and hot chlorine-containing solvents. Polymers were verified by elemental analysis. The number-average molecular weights (M_n) and polydispersity index (PDI) of the polymers were determined by gel-permeation chromatography (GPC) with trichlorobenzene as an eluent. The GPC plots are shown in Fig. S1 (ESI†) and the

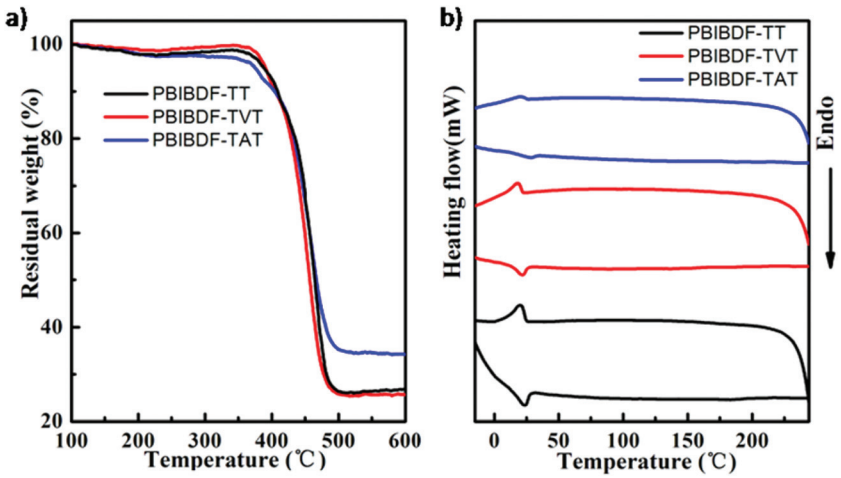

Fig. 1 TGA and DSC plots of three BIBDF-based polymers.

corresponding data are also listed in Table S1.† The number-average molecular weights were 26.47 kDa (PDI = 1.65) for **PBIBDF-TT**, 28.07 kDa (PDI = 1.72) for **PBIBDF-TVT**, and 23.95 kDa (PDI = 1.83) for **PBIBDF-TAT**.

The thermogravimetric analysis (TGA) and differential scanning calorimetry (DSC) curves of the three BIBDF-based polymers are shown in Fig. 1 and the decomposition temperatures (T_d) are collected in Table S1.† The temperatures of 5% weight-loss were chosen as the onset point of decomposition, which were thermally stable up to temperatures of 375–389 °C. The thermal-stability of the three polymers was adequate for application in optoelectronic devices. DSC curves clearly showed endothermic peaks at 22–24 °C during heating up, and corresponding exothermic peaks at 19–20 °C were also observed when they were cooled down. The same transition temperatures of the three polymers should be attributed to the phase transition temperature caused by the melting of the long alkyl chains.[8b]

2.2. Optical properties

The normalized UV-vis-NIR absorption spectra of these three BIBDF-based polymers in dilute chloroform solutions and as thin films casted from chloroform are shown in Fig. 2. Polymers displayed typical dual-bands consisting of sharp ones at the high energy region and more intense, broader ones with additional shoulder peaks at the low energy region. As listed in Table 1, the absorption maxima (λ_{max}^{abs}) of **PBIBDF-TT**, **PBIBDF-TVT** and **PBIBDF-TAT** in a chloroform solution were located at 827, 835 and 780 nm, respectively. From the solution state to a solid film, the λ_{max}^{abs} of the three polymers showed small red-shifts of about 8–11 nm. The absence of strong red-shifts from solution to film could be ascribed to the probable pre-aggregation in solution.[9] The absorption of **PBIBDF-TAT** was blue-shifted compared with those of **PBIBDF-TT** and **PBIBDF-TVT**; this is because the triple bond is electron-withdrawing and indicates that the triple bond as a linker results in a weaker donor compared to the single bond/double bond

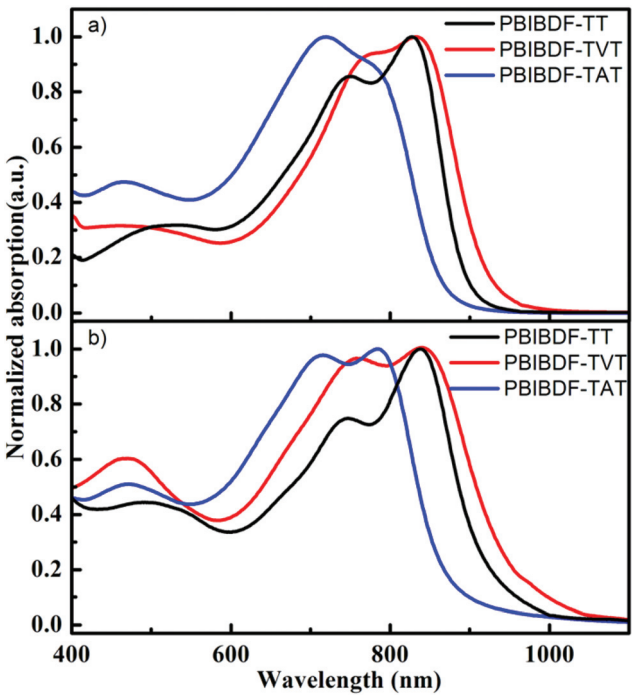

Fig. 2 Normalized absorption spectra of three BIBDF-based polymers in chloroform solution (a) and in solid film (b).

as a linker.[10] The edges of the film absorption bands for **PBIBDF-TT**, **PBIBDF-TVT** and **PBIBDF-TAT** were at 968, 1015, and 906 nm, respectively. The corresponding optical bandgaps of **PBIBDF-TT**, **PBIBDF-TVT** and **PBIBDF-TAT** were 1.28, 1.22, and 1.37 eV, respectively. The narrow bandgaps were due to the extended π-conjugation along the polymer backbone as well as strong intramolecular and intermolecular interactions.[8d]

2.3. Electrochemical properties

The LUMO and HOMO energy levels of polymers, which are closely related to the transport characteristics of OTFTs, can be

Table 1 Optical and electrochemical properties of the three BIBDF-based polymers

Polymer	λ_{max}^{abs} (nm) Solution	λ_{max}^{abs} (nm) Film	λ_{onset}^{abs} Film	$E_g^{opt\ a}$ (eV)	HOMO^b (eV)	LUMO^b (eV)	$E_g^{ec\ c}$ (eV)
PBIBDF-TT	827	838	968	1.28	−5.57	−4.10	1.47
PBIBDF-TVT	835	844	1015	1.22	−5.43	−4.09	1.34
PBIBDF-TAT	716 (780)	788	906	1.37	−5.60	−4.11	1.49

^{a} $E_g^{opt} = 1240/\lambda_{onset}^{abs}$ (in film). ^{b} HOMO = −(4.75 + E_{onset}^{ox}), LUMO = −(4.75 + E_{onset}^{red}). ^{c} E_g^{ec} = −(HOMO–LUMO).

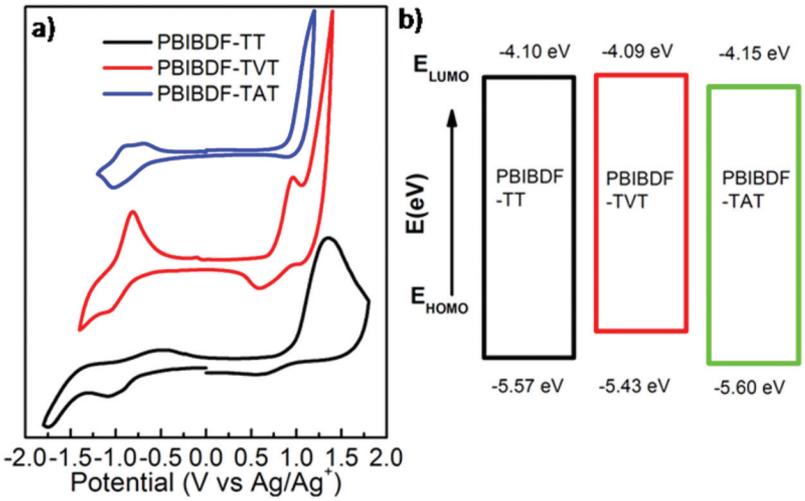

Fig. 3 Cyclic voltammograms of polymer thin films and energy level diagrams.

determined by cyclic voltammetry (CV). The cyclic voltammograms of the three polymers as thin films are shown in Fig. 3a. The electrochemical data are summarized in Table 1 and are schematically depicted in Fig. 3b. The potentials were referenced to Ag/Ag^+ and the redox Fc/Fc^+ was assumed at an absolute energy level of 4.8 eV to vacuum. The redox Fc/Fc^+ was measured under the same conditions as polymer thin-films and was located at 0.05 V related to the Ag/Ag^+ electrode. As listed in Table 1, the oxidation onset potentials (E_{onset}^{ox}) of **PBIBDF-TT**, **PBIBDF-TVT**, and **PBIBDF-TAT** were 0.82, 0.68, and 0.85 V, corresponding to the HOMO energy levels of −5.57, −5.43, and −5.60 eV, respectively. **PBIBDF-TVT** had a slightly higher HOMO energy level than those of the other two polymers because of the existence of the relatively strong donating (*E*)-2-(2-(thiophen-2-yl)vinyl)thiophene. The onset reduction potentials (E_{onset}^{red}) of **PBIBDF-TT**, **PBIBDF-TVT**, and **PBIBDF-TAT** were located at −0.65, −0.64, and −0.66 V. The three polymers had almost the same E_{onset}^{red} and correspondingly showed similar LUMO energy levels of −4.10, −4.09, and −4.11 eV, because typically the LUMO energy levels were controlled by the LUMO level of the acceptor unit.[11] The electrochemical bandgaps estimated from the difference between the HOMO and LUMO energy levels were 1.34–1.49 eV, which were about 0.12–0.19 eV larger than the corresponding optical bandgaps, probably due to the interfacial barrier for charge injection.[12] Judging from the HOMO and LUMO energy levels of BIBDF-based polymers, the three polymers should be suitable candidates as n-channel semiconductors for the injection, accumulation, and transport of electrons when an appropriate single metal (such as Au) is used.

2.4. OTFT performance

Bottom-gate/top-contact transistors were fabricated based on the polymers as semiconductor layers. The evaluation of OTFTs was carried out under vacuum (3×10^{-4} mbar). First, polymer thin-films were prepared on a conventional octadecyltrichlorosilane (OTS)-modified SiO_2/Si substrate by spin coating. As shown in Fig. S2,† the three polymers displayed clear n-channel transport characteristics and their electrical properties are summarized in Table 2. It is well known that fluoropolymer Cytop surfaces were most suitable for upper-deposited semiconductors, especially for Cytop-modified surfaces which are themselves hydroxyl-group-free and hydrophobic.[7a,13] Therefore, we also fabricated OTFTs based on the polymers on Cytop-modified SiO_2/Si substrates. The mobilities of the non-annealed (N/A) devices of **PBIBDF-TT**, **PBIBDF-TVT**, and **PBIBDF-TAT** were 0.18, 0.18, and 0.04 $cm^2\ V^{-1}\ s^{-1}$ (Fig. S3†), respectively.

As far as the n-type solution processable semiconductors, annealing of the polymer films generally provides an excellent approach for achieving an ordered film. The thermal-annealing can improve the crystallinity of the films while significantly

Table 2 OTFT performances of the three BIBDF-based polymers

		n-Channel[a]			
Dielectric layer	Annealing temperature [°C]	$\mu_{e,max}$ ($cm^2\ V^{-1}\ s^{-1}$)	$\mu_{e,avg}$[b] ($cm^2\ V^{-1}\ s^{-1}$)	I_{on}/I_{off}[c]	V_{th} (V)
	PBIBDF-TT				
(OTS/SiO_2)	rt	0.12	0.11 ± 0.011	3.0×10^5	6.3
($Cytop/SiO_2$)	rt	0.18	0.13 ± 0.031	3.6×10^4	23.8
	150	0.65	0.48 ± 0.124	5.5×10^4	43.1
	180	0.45	0.30 ± 0.085	1.1×10^4	30.3
	210	0.10	0.06 ± 0.021	1.9×10^4	21.8
	PBIBDF-TVT				
(OTS/SiO_2)	rt	0.11	0.09 ± 0.018	4.2×10^4	30.9
($Cytop/SiO_2$)	rt	0.18	0.16 ± 0.020	3.1×10^5	41.9
	150	0.25	0.19 ± 0.046	2.2×10^5	41.9
	180	0.55	0.44 ± 0.096	1.4×10^5	41.6
	PBIBDF-TAT				
(OTS/SiO_2)	rt	0.03	0.02 ± 0.004	1.2×10^5	25.3
($Cytop/SiO_2$)	rt	0.04	0.03 ± 0.006	3.9×10^5	37.9
	150	0.07	0.05 ± 0.012	1.9×10^5	36.8
	180	0.13	0.08 ± 0.025	4.6×10^5	29.9

[a] The evaluation of OTFTs were carried out under vacuum (3×10^{-4} mbar). [b] Average mobility from more than 8–10 devices. [c] Evaluated at V_{DS} = 80 V.

decreasing the effect of the residual solvent on the carrier transport, resulting in high mobility.[14] The representative output and transfer characteristics of the OTFTs based on the polymers are shown in Fig. 4 and the calculated field-effect performances are listed in Table 2. The optimal annealing temperatures were 150 °C for **PBIBDF-TT** and 180 °C for **PBIBDF-TVT** and **PBIBDF-TAT**. For the **PBIBDF-TT** system, the highest electron mobility of 0.65 $cm^2\ V^{-1}\ s^{-1}$ with an I_{on}/I_{off} of 5.5×10^4 was obtained after 150 °C annealing. At a higher annealing temperature of 180 °C, the mobilities dropped slightly to 0.45 $cm^2\ V^{-1}\ s^{-1}$. With further increasing the annealing temperature to 210 °C, the mobilities dropped dramatically to 0.10 $cm^2\ V^{-1}\ s^{-1}$. The worse mobility at 210 °C annealing might be attributed to the thermal-decomposition of large side-chains as evidenced by the TGA curve. For **PBIBDF-TVT**, the as-cast thin films exhibited a moderate mobility of 0.18 $cm^2\ V^{-1}\ s^{-1}$. With thermal annealing, the mobility of **PBIBDF-TVT** thin films increased, and the highest mobility was 0.55 $cm^2\ V^{-1}\ s^{-1}$ after thermal annealing at 180 °C. The **PBIBDF-TAT**-based devices displayed the lowest mobility among the three polymers with the highest mobility of 0.13 $cm^2\ V^{-1}\ s^{-1}$ after thermal annealing at 180 °C. No hole transport was observed for the three polymers under vacuum (3×10^{-4} mbar). This is presumably due to the large hole injection barrier between their low-lying HOMO levels and the work function of gold (~4.7–5.1 eV) under vacuum (3×10^{-4} mbar) conditions. Another BIBDF-based polymer (**PBIBDF-BT**), which was reported in our previous paper, could also exhibit n-channel transport under these vacuum conditions.[8a]

OTFTs' environmental stability for **PBIBDF-TT** and **PBIBDF-TVT** was also monitored over the course of storage under ambient conditions, and the relevant OTFT performances (electron mobility and I_{on}/I_{off}) are displayed in Fig. 5. After 70 days' air exposure, the highest mobilities of **PBIBDF-TT** and **PBIBDF-TVT** still remained at the values of 0.33 and 0.31 $cm^2\ V^{-1}\ s^{-1}$, respectively. Moreover, the I_{on}/I_{off} of the two polymers remained over 10^4 in the whole course of storage under ambient conditions. **PBIBDF-TT** and **PBIBDF-TVT** thin-films showed robust storage stability, which was doubtless attributed to the low-lying LUMO and HOMO energy levels created by the strong electron-deficient **BIBDF** unit. The other reason might probably be due to close π–π stacking distance that was also beneficial to defend the diffusion of water and oxygen (see below). However, the mobilities of the three polymers were lower than those of the reported BIBDF-based polymers.[8a–c] The main reason may be ascribed to the relatively low molecular weight of the three BIBDF-based polymers, which significantly influences the OTFTs' performances. The polymer semiconductors with high molecular weight usually showed high field-effect performance compared with that of the lower molecular weight ones.[15] For BIBDF containing polymers, the reported polymer with the highest mobility so far had an M_n of 77.2 kDa,[8b] while the **PBIBDF-TT** with a mobility of 0.65 $cm^2\ V^{-1}\ s^{-1}$ showed an M_n of only 26.5 kDa. Further optimizations of the molecular weight of **PBIBDF-TT** and **PBIBDF-TVT** for the improvement of the electron mobility are in progress.

2.5. Thin-film microstructure analysis

To elucidate the structure–property relationships in the three BIBDF-based polymers, grazing incident X-ray diffraction (GIXD) and taping mode atomic force microscopy (AFM) were employed to investigate the crystalline nature, molecular orientation, and morphologies of the three polymer films. The 2D-GIXD images and the corresponding diffractogram profiles of the films with and without annealing are shown in Fig. 6

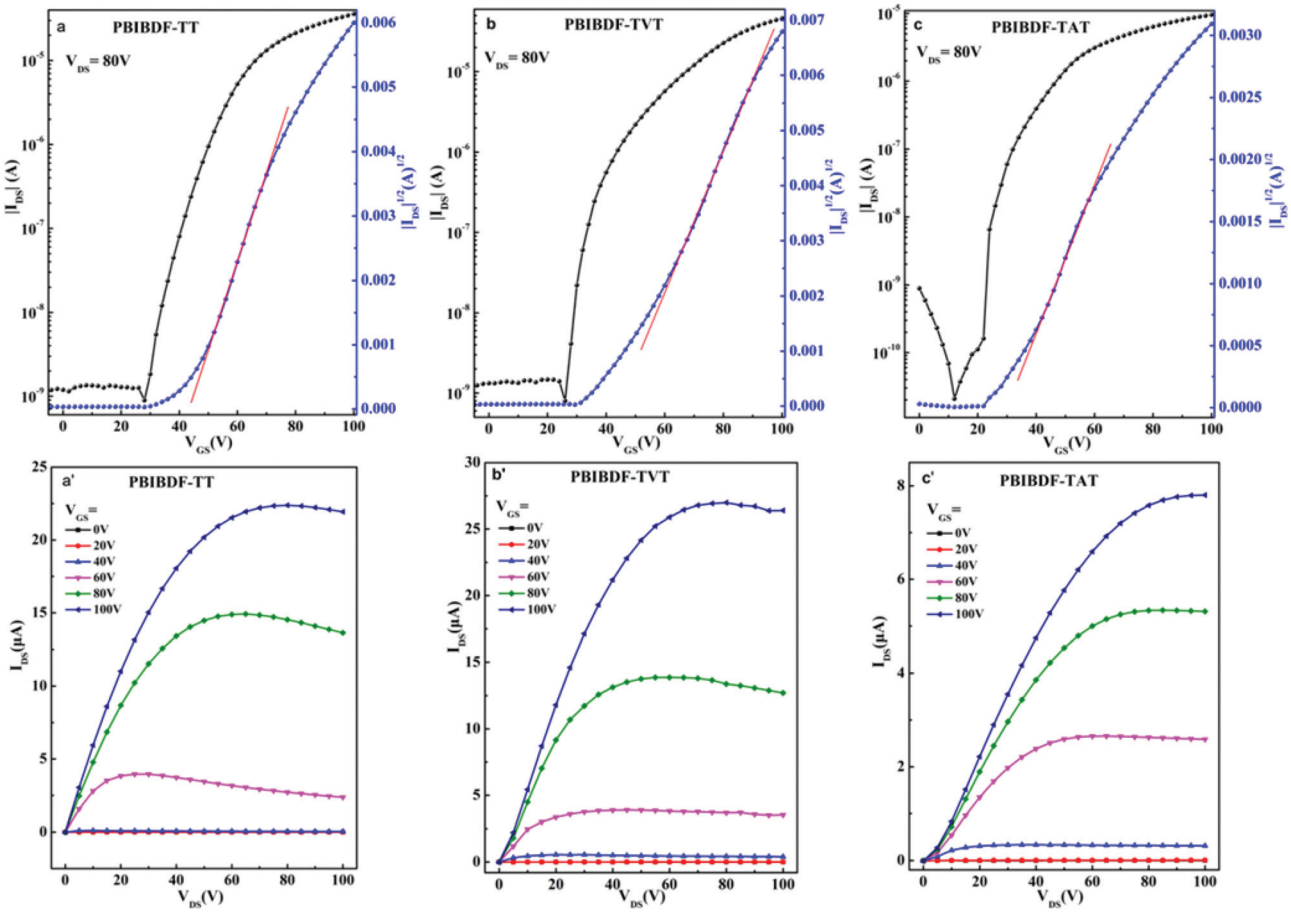

Fig. 4 Typical transfer and output characteristics of OTFT devices based on polymer films coated on Cytop-modified SiO_2/Si substrates at an optimized annealing temperature of 150 or 180 °C.

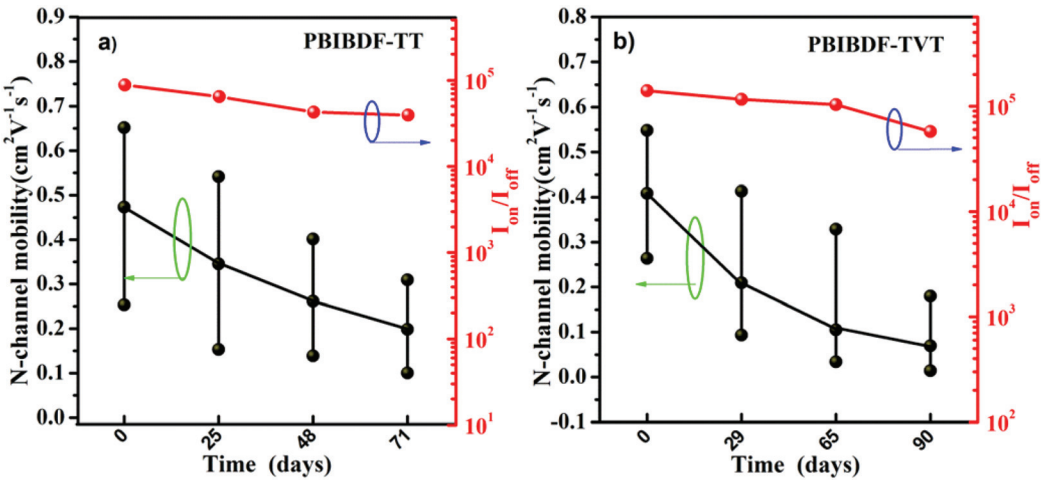

Fig. 5 OTFT performances (electron and I_{on}/I_{off}) for **PBIBDF-TT** and **PBIBDF-TAT** after exposure to air.

and Fig. S4.† The crystallographic parameters are listed in Table S2.† For **PBIBDF-TT** and **PBIBDF-TVT** thin films, the non-annealing (N/A) films showed out-of-plane reflection peaks (100) and well defined (200), (300), and (400) diffraction peaks along the out-of-plane q_z axis. Compared with the N/A films, the annealing films for **PBIBDF-TT** and **PBIBDF-TVT** exhibited more and stronger diffraction peaks (highly ordered (100)–(500)). The presence of highly ordered reflection peaks

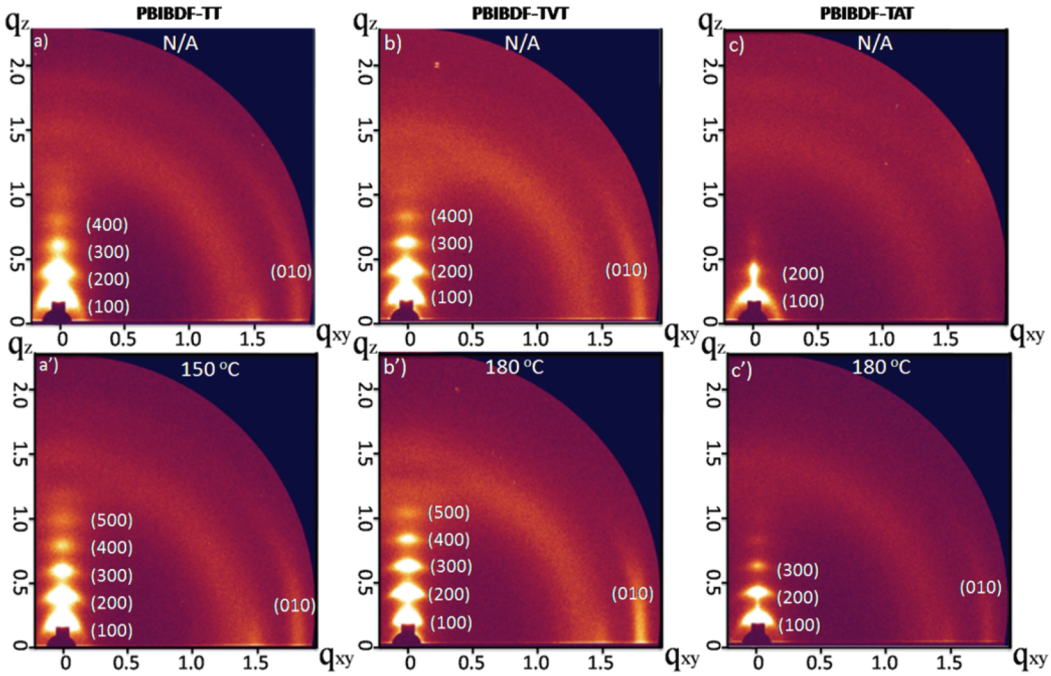

Fig. 6 GIXD patterns of polymer films coated on Cytop-modified SiO_2/Si substrates with and without annealing.

of N/A and annealing films suggested that **PBIBDF-TT** and **PBIBDF-TVT** had long-range ordered, lamellar crystalline structures. In contrast, the **PBIBDF-TAT** thin film displayed relatively poor molecular ordering among the three polymers with defined (100), (200), and (300) diffraction peaks after annealing at 180 °C. The lamellar spacings were 28.96 Å for **PBIBDF-TT**, 29.45 Å for **PBIBDF-TVT**, and 29.83 Å for **PBIBDF-TAT**, which were calculated from their (100) peaks at q_z = 0.217, 0.213, and 0.211 $Å^{-1}$. The observed interlayer distances were much shorter than the molecular modeled length of alkyl chains, suggesting that the alkyl chains were not fully extended in the films when coated on the substrates even in the presence of thermal annealing. However, the non-fully extended alkyl chains did not hinder the co-planarity of the main chain. Besides out-of-plane peaks, the in-plane XRD spectra of **PBIBDF-TT** and **PBIBDF-TVT** also displayed the (010) reflection peaks in the case of films of both N/A and annealing conditions. These results suggested clearly that the films of **PBIBDF-TT** and **PBIBDF-TVT** favored edge-on orientation on the substrate, thus facilitating efficient charge carrier hopping transport. In contrast, the N/A film of **PBIBDF-TAT** did not show any discernible peak in the q_{xy} plane, while the annealed film revealed a weak peak centered in the q_{xy} plane. The (010) diffraction peaks were located at q_{xy} = 1.82, 1.79, and 1.80 $Å^{-1}$ for **PBIBDF-TT**, **PBIBDF-TVT**, and **PBIBDF-TAT**, respectively, so the π–π stacking distances were 3.45 Å for **PBIBDF-TT**, 3.51 Å for **PBIBDF-TVT**, and 3.49 Å for **PBIBDF-TAT** (Fig. S5†). The calculated π–π stacking distances of the three polymers were slightly smaller than those of the reported BIBDF-based polymers,[8a–c] and even much lower than those of the famous high performance DPP-based polymer **PDVT-10** (3.66 Å) and **PDVT-8** (3.78 Å).[3b] The remarkable close π–π distance between polymer backbones suggested that strong intermolecular interactions exist. Charge transport of the conjugated polymer is highly dependent on the intermolecular overlap integral. However, the annealed **PBIBDF-TAT** thin film with the close π–π stacking distance also showed miserable performance because of the poor crystalline structures among the three polymers. The close π–π distance and the long-range ordered, lamellar crystalline structures both contributed to the high charge carrier mobilities for **PBIBDF-TT** and **PBIBDF-TVT**.

The AFM height images of the three polymer thin films are also shown in Fig. 7. For **PBIBDF-TT** and **PBIBDF-TVT**, the N/A films showed fine, clustered and nano-fibrillar crystals in the whole area. Such crystalline networks were presumably caused by strong intermolecular interactions. As annealed at 150 or 180 °C, the two polymer films both exhibited larger polycrystalline grains than the N/A films, leading to fewer grain boundaries and therefore higher field effect performance. Further increasing the annealing temperature to 210 °C, the degradation of the large alkyl chains gave rise to large circular domains in the film, which was responsible for the decline in device performance (Fig. S6†). On the other hand, the N/A thin film of **PBIBDF-TAT** showed isolated grains with large grain boundaries. At an annealing temperature of 180 °C, the film became well interconnected. The annealed **PBIBDF-TAT** thin film, however, had poor crystalline networks compared with those of the other two polymer films, which was also responsible for the lowest mobilities among the three BIBDF-based polymers.

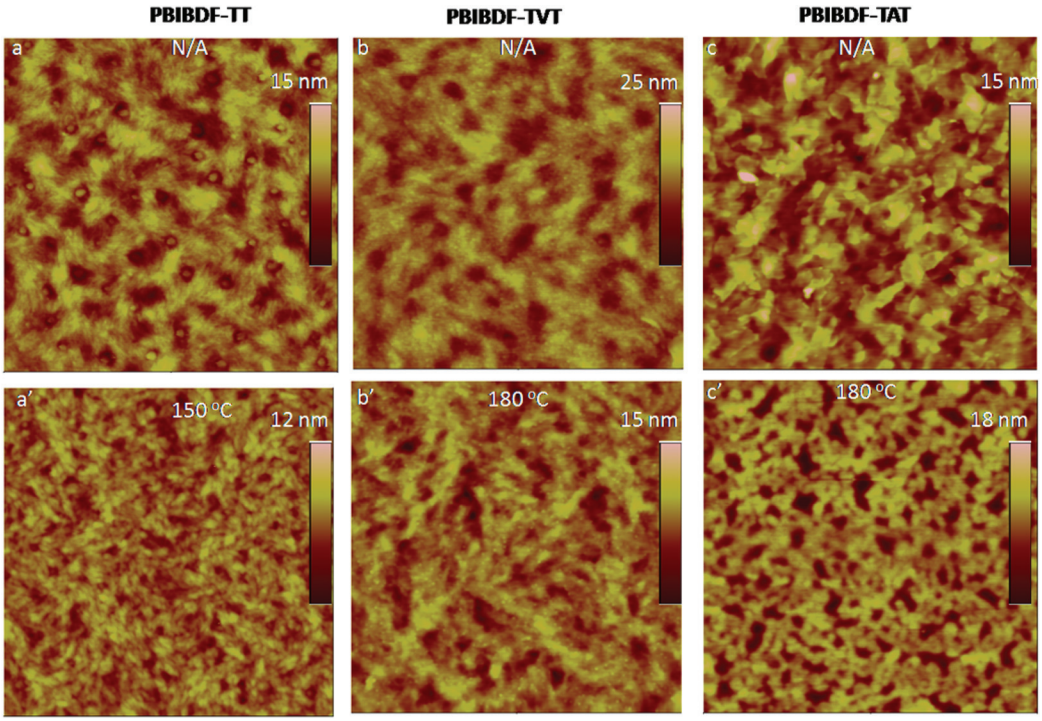

Fig. 7 AFM topography images (2 μm × 2 μm) of polymer films coated on Cytop-modified SiO_2/Si substrates with and without annealing.

3. Conclusion

In this work, new BIBDF-based polymers with three different donors were designed and synthesized. These three polymers showed almost the same LUMO energy levels (<−4.0 eV) while they had different crystalline structures in thin-films and varied π–π stacking distances observed in the GIXD characterization. OTFTs based on the three polymers with common architectures and their environmental stability were also investigated. The results indicated that thermal annealing had a substantial influence on crystalline nature, morphologies as well as charge transport. **PBIBDF-TT** with long-range ordered, lamellar crystalline structure and close π–π stacking distance showed an electron mobility of 0.65 $cm^2\ V^{-1}\ s^{-1}$ with a high I_{on}/I_{off} value of over 10^4, which was the highest one in the three polymers. On the other hand, because of the poor crystalline structure, **PBIBDF-TAT** displayed a miserable electron mobility of 0.13 $cm^2\ V^{-1}\ s^{-1}$ though the polymer thin film also had a similar π–π stacking distance. Overall, these results suggest that (i) BIBDF is a promising building block for constructing high performance electron transport materials; (ii) the donor unit has a significant effect on BIBDF-based polymers and the field-effect performances can be effectively optimized by introducing different donor units; (iii) the conjugated polymer with not only close π–π stacking distance but also long-range ordered lamellar crystalline structure as well as high molecular weight would show satisfactory OTFT performance.

4. Experimental

4.1. Characterization

Nuclear magnetic resonance (NMR) spectra were recorded using a Mercury plus 600 MHz machine. Elemental analysis of the polymer was performed using a Vario EL instrument. Molecular weights of the polymers were determined by gel permeation chromatography (GPC) analyses on a Waters Series 1525 gel using 1,2,4-trichlorobenzene as an eluent with polystyrene as standards. Thermo-gravimetric analyses (TGA) were conducted with a TA Instruments QS000IR at a heating rate of 10 °C min^{-1} under nitrogen gas flow. Differential scanning calorimetry (DSC) was conducted under nitrogen using a TA Instruments Q2000. The sample (about 5 mg in weight) was first cooled down to −25 °C, then heated up to 250 °C and held for 2 min to remove thermal history, followed by cooling at a rate of 10 °C min^{-1} to −25 °C and then heating at a rate of 10 °C min^{-1} to 250 °C in all cases. UV-vis-NIR absorption spectra were recorded on polymer solutions in chloroform and polymer films cast onto quartz glass using a Perkin-Elmer model λ 20 UV-vis-NIR spectrophotometer. CV measurements were conducted on a CHI 660D electrochemical analyzer under nitrogen in a solution containing tetra-*n*-butylammonium hexafluorophosphate (0.1 M) in deoxygenated anhydrous acetonitrile at a scan rate of 100 mV s^{-1}. The platinum electrode was used as both the working electrode and the auxiliary electrode, and an Ag/Ag^+ electrode was used as a reference electrode. Polymer thin films were coated on the surface of the platinum electrode and ferrocene was chosen as a reference.

Grazing-incidence X-ray diffraction (GIXD) studies were performed using 3C beamlines at the Pohang Accelerator Laboratory (PAL) in Korea. The atomic force microscope (AFM) measurements were performed on polymer thin films on a Cytop-modified SiO_2/Si substrate using an SPA300HV instrument with an SPI3800 controller (Seiko Instruments).

4.2. Fabrication and characterization of field-effect transistors

Bottom-gate/top-contact OTFT devices were fabricated on a common gate of highly n-doped silicon with a 300 nm thick thermally grown SiO_2 dielectric layer. A fluoropolymer Cytop was spin-coated onto an SiO_2 dielectric layer (~20 nm). A chloroform solution containing a semiconductor polymer (5 mg mL^{-1}) was dropped onto the Cytop (or OTS) thin film and spin-coated. The polymer films were subsequently annealed at 150, 180 and 210 °C for 30 min under a nitrogen atmosphere. Then Au source–drain electrodes were evaporated on top of the semiconductor layers (56 nm). The OTFT devices had a channel length (L) of 100 μm and a channel width (W) of 800 μm. The evaluation of the OTFTs was performed in a vacuum (3×10^{-4} mbar) using a Keithley 4200 parameter on the probe stage. The mobilities for electrons (μ_e) were obtained using the following equation used at the saturation regime: $I_d = (W/2L)C_i\mu_e(V_g - V_{th})^2$, where W/L is the channel width/length, I_d is the drain current in the saturated regime, C_i is the capacitance of Cytop/SiO_2 gate-dielectric, and V_{th} is the threshold voltage.

4.3. Materials

6-Bromoindoline-2,3-dione was obtained from Darui Chemical Co. Ltd, Shanghai, China. Other chemicals used in this work were purchased from Sigma-Aldrich Chemical Company, Alfa Aesar Chemical Company and Sinopharm Chemical Reagent Co. Ltd, China. All commercially available reagents were used without further purification. Tetrahydrofuran (THF) and toluene were freshly distilled over a sodium wire under nitrogen prior to use. 2,5-Bis(trimethylstannyl)thieno[3,2-*b*]thiophene (**M1**), 1,2-bis(5-(trimethylstannyl)-thiophene-2-yl)ethane (**M2**) and 1,2-bis(5-(trimethylstannyl)-thiophene-2-yl)ethyne (**M3**) were synthesized *via* published procedures.[3b,10c,16]

4.4. Synthesis of monomers and polymers

Synthesis of compound 1. To a solution of 2,5-dihydroxy-1,4-benzenediacetic acid (5.6 g, 24.79 mmol) in toluene (60 mL) under a nitrogen atmosphere, acetic anhydride (100 mL) was added. The reaction mixture was refluxed for 4 hours. After removing the solvent, the crude product was washed with hot alcohol. A white precipitate formed, which was used in the next step without any further purification.

Synthesis of compound 2. Anhydrous potassium carbonate (6.36 g, 45.99 mmol) and 6-bromoindoline-2,3-dione (2.65 g, 11.73 mmol) were dissolved in anhydrous *N*,*N*-dimethylformamide (DMF, 50 mL) at 70 °C under a nitrogen atmosphere, after vigorous stirring for 1 h. 4-Bromo-alkyl (9.04 g, 14.08 mmol) was added dropwise and the mixture was kept under stirring and heated overnight at 70 °C. After cooling to room temperature, the solution was poured into water (300 mL) and then extracted with dichloromethane. The organic layer was collected and dried with anhydrous sodium sulfate. Solvent was removed under reduced pressure and the residue was purified by flash chromatography on silica gel with petroleum–dichloromethane–diethyl ether (15 : 1 : 1) as an eluent to give the title compound (6.52 g, 55.8%). The compound was used in the next step without any further purification.

Synthesis of BIBDF. Compound **1** (0.77 g, 4.06 mmol), compound **2** (6.40 g, 8.13 mmol), and toluenesulfonic acid (TsOH, 0.22 g, 1.14 mmol) were stirred in acetic acid (40 mL) under a nitrogen atmosphere. The mixture was refluxed for 17 h under nitrogen. The reaction mixture was then cooled to room temperature and filtered. The solid was washed with methanol. The crude product was further purified by column chromatography on silica gel using dichloromethane–petroleum ether (1 : 1) as an eluent to obtain the title compound (3.23 g, 45.0%). ^{1}H NMR (600 MHz, $CDCl_3$, ppm): δ = 9.08 (s, 2H), 8.90 (d, 2H), 7.17 (d, 2H), 6.91 (s, 2H), 3.71 (d, 4H), 1.68 (s, 4H), 1.20–1.35 (m, 142H), 0.86 (t, 12H).

Synthesis of PBIBDF-TT. 2,5-Bis(trimethylstannyl)thieno-[3,2-*b*]thiophene (0.065 g, 0.14 mmol), **BIBDF** (0.24 g, 0.14 mmol), $Pd_2(dba)_3$ (0.0042 g, 0.0046 mmol), P(*o*-tol)$_3$ (0.012 g, 0.038 mmol) and degassed toluene (8 mL) were added to a Schlenk tube. The solution was subjected to three cycles of evacuation and admission of nitrogen. The mixture was stirred at 110 °C for 48 h. After cooling down to room temperature, the mixture was poured into methanol (100 ml) and stirred for 2 h. A black precipitate was collected by filtration. The product was purified through Soxhlet extraction using methanol and dichloromethane to remove oligomers and other impurities. The remaining polymer was extracted with hot chloroform in an extractor for 24 h. After removing the solvent, a black solid was collected (0.22 g, 71.7%). Elemental analysis: calcd for $(C_{112}H_{174}N_2O_6S_2)_n$ (%): C, 78.80, H, 10.18, N, 1.64, found (%): C, 78.68, H, 9.88, N, 1.49. GPC: M_n = 26.5 kDa, PDI = 1.65.

Synthesis of PBIBDF-TVT and PBIBDF-TAT. The same procedures were used as those for **PBIBDF-TT**. The compounds used were $Pd_2(dba)_3$ (0.0042 g, 0.0046 mmol), P(*o*-tol)$_3$ (0.012 g, 0.038 mmol), **BIBDF** (0.24 g, 0.14 mmol), **M2** (0.073 g, 0.14 mmol) or **M3** (0.072, 0.14 mmol). After workup, black polymers were obtained.

PBIBDF-TVT: yield: 0.27 g, 85.6%. Elements analysis: calculated for $(C_{116}H_{178}N_2O_6S_2)_n$ (%): C, 79.13, H, 10.19, N, 1.59, found (%): C, 79.04, H, 9.65, N, 1.45. GPC: M_n = 28.07 kDa, PDI = 1.72.

PBIBDF-TAT: yield: 0.10 g, 39.1%. Elements analysis: calculated for $(C_{116}H_{176}N_2O_6S_2)_n$ (%): C, 79.22, H, 10.09, N, 1.59, found (%): C, 79.09, H, 9.93, N, 1.45. GPC: M_n = 23.95 kDa, PDI = 1.83.

Acknowledgements

This work was supported by the Major State Basic Research Development Program of China (2012CB723406), the National

Nature Science Foundation of China (NSFC grant no. 21204017, 61107014, 51103034, and 21174036), and the Program for New Century Excellent Talents in University (NCET-12-0839). The authors thank 3C beamlines (the Pohang Accelerator Laboratory in Korea) for providing the beam time.

References

1 (*a*) P. F. Moonen, I. Yakimets and J. Huskens, *Adv. Mater.*, 2012, **24**, 5526–5541; (*b*) A. Tsumura, H. Koezuka and T. Ando, *Appl. Phys. Lett.*, 1986, **49**, 1210–1212; (*c*) H. T. Yi, M. M. Payne, J. E. Anthony and V. Podzorov, *Nat. Commun.*, 2012, **3**, 1259, 1–6; (*d*) S. Holliday, J. E. Donaghey and I. McCulloch, *Chem. Mater.*, 2013, **26**, 647–663.

2 (*a*) X. Guo, A. Facchetti and T. J. Marks, *Chem. Rev.*, 2014, **114**, 8943–9021; (*b*) Y. F. Li, *Acc. Chem. Res.*, 2012, **45**, 723–733; (*c*) X. Guo, S. R. Puniredd, M. Baumgarten, W. Pisula and K. Müllen, *Adv. Mater.*, 2013, **25**, 5467–5472; (*d*) Q. Wu, M. Wang, X. Qiao, Y. Xiong, Y. Huang, X. Gao and H. Li, *Macromolecules*, 2013, **46**, 3887–3894; (*e*) G. Zhang, Y. Fu, Z. Xie and Q. Zhang, *Macromolecules*, 2011, **44**, 1414–1420; (*f*) C. Duan, F. Huang and Y. Cao, *J. Mater. Chem.*, 2012, **22**, 10416–10434.

3 (*a*) H.-R. Tseng, H. Phan, C. Luo, M. Wang, L. A. Perez, S. N. Patel, L. Ying, E. J. Kramer, T.-Q. Nguyen, G. C. Bazan and A. J. Heeger, *Adv. Mater.*, 2014, **26**, 2993–2998; (*b*) H. Chen, Y. Guo, G. Yu, Y. Zhao, J. Zhang, D. Gao, H. Liu and Y. Liu, *Adv. Mater.*, 2012, **24**, 4618–4622; (*c*) J. Li, Y. Zhao, H. Tan, Y. Guo, C. Di, G. Yu, Y. Liu, M. Lin, S. Lim, Y. Zhou, H. Su and B. Ong, *Sci. Rep.*, 2012, **2**, 754, 1–9.

4 (*a*) L. Peng, L. Hu and X. Fang, *Adv. Mater.*, 2013, **25**, 5321–5328; (*b*) R. Di Pietro and H. Sirringhaus, *Adv. Mater.*, 2012, **24**, 3367–3372.

5 (*a*) T. D. Anthopoulos, G. C. Anyfantis, G. C. Papavassiliou and D. M. de Leeuw, *Appl. Phys. Lett.*, 2007, **90**, 122105; (*b*) A. Facchetti, *Chem. Mater.*, 2010, **23**, 733–758.

6 (*a*) P.-T. Wu, T. Bull, F. S. Kim, C. K. Luscombe and S. A. Jenekhe, *Macromolecules*, 2009, **42**, 671–681; (*b*) D. Chen, Y. Zhao, C. Zhong, S. Gao, G. Yu, Y. Liu and J. Qin, *J. Mater. Chem.*, 2012, **22**, 14639–14644; (*c*) Y. Wen and Y. Liu, *Adv. Mater.*, 2010, **22**, 1331–1345.

7 (*a*) J. H. Park, E. H. Jung, J. W. Jung and W. H. Jo, *Adv. Mater.*, 2013, **25**, 2583–2588; (*b*) H. Yan, Z. Chen, Y. Zheng, C. Newman, J. R. Quinn, F. Dotz, M. Kastler and A. Facchetti, *Nature*, 2009, **457**, 679–686; (*c*) X. Zhan, Z. a. Tan, B. Domercq, Z. An, X. Zhang, S. Barlow, Y. Li, D. Zhu, B. Kippelen and S. R. Marder, *J. Am. Chem. Soc.*, 2007, **129**, 7246–7247.

8 (*a*) G. Zhang, P. Li, L. Tang, J. Ma, X. Wang, H. Lu, B. Kang, K. Cho and L. Qiu, *Chem. Commun.*, 2014, **50**, 3180–3183; (*b*) T. Lei, J. H. Dou, X. Y. Cao, J. Y. Wang and J. Pei, *Adv. Mater.*, 2013, **25**, 6589–6593; (*c*) T. Lei, J.-H. Dou, X.-Y. Cao, J.-Y. Wang and J. Pei, *J. Am. Chem. Soc.*, 2013, **135**, 12168–12171; (*d*) Z. Yan, B. Sun and Y. Li, *Chem. Commun.*, 2013, **49**, 3790–3792; (*e*) J.-H. Dou, Y.-Q. Zheng, T. Lei, S.-D. Zhang, Z. Wang, W.-B. Zhang, J.-Y. Wang and J. Pei, *Adv. Funct. Mater.*, 2014, **24**, 6270–6278; (*f*) T. Lei, J.-Y. Wang and J. Pei, *Acc. Chem. Res.*, 2014, **47**, 1117–1126.

9 (*a*) J. Kim, A.-R. Han, J. Hong, G. Kim, J. Lee, T. J. Shin, J. H. Oh and C. Yang, *Chem. Mater.*, 2014, **26**, 4933–4942; (*b*) N. Zhou, X. Guo, R. P. Ortiz, S. Li, P. R. Chang, A. Facchetti and T. Marks, *Adv. Mater.*, 2012, **24**, 2242–2248; (*c*) J. Kim and T. swager, *Nature*, 2001, **411**, 1030–1034.

10 (*a*) W. A. Braunecker, S. D. Oosterhout, Z. R. Owczarczyk, R. E. Larsen, B. W. Larson, D. S. Ginley, O. V. Boltalina, S. H. Strauss, N. Kopidakis and D. C. Olson, *Macromolecules*, 2013, **46**, 3367–3375; (*b*) P. M. Beaujuge, S. V. Vasilyeva, S. Ellinger, T. D. McCarley and J. R. Reynolds, *Macromolecules*, 2009, **42**, 3694–3706; (*c*) H.-J. Yun, H. Choi, S.-K. Kwon, Y.-H. Kim and K. Cho, *Chem. Mater.*, 2014, **26**, 3928–3937.

11 J. Chen and Y. Cao, *Acc. Chem. Res.*, 2009, **42**, 1709–1718.

12 (*a*) L. Huo, H.-Y. Chen, J. Hou, T. L. Chen and Y. Yang, *Chem. Commun.*, 2009, 5570–5572; (*b*) X. Hu, W. Fu, L. Zuo, H. Shi, M. Chen, S. Liu, J. Pan, L. Fu, M. Shi and H. Chen, *Tetrahedron*, 2013, **69**, 3419–3424.

13 W. L. Kalb, T. Mathis, S. Haas, A. F. Stassen and B. Batlogg, *Appl. Phys. Lett.*, 2007, **90**, 092104.

14 (*a*) S. Handa, E. Miyazaki, K. Takimiya and Y. Kunugi, *J. Am. Chem. Soc.*, 2007, **129**, 11684–11685; (*b*) J. A. Letizia, M. R. Salata, C. M. Tribout, A. Facchetti, M. A. Ratner and T. J. Marks, *J. Am. Chem. Soc.*, 2008, **130**, 9679–9694.

15 H.-R. Tseng, L. Ying, B. B. Y. Hsu, L. A. Perez, C. J. Takacs, G. C. Bazan and A. J. Heeger, *Nano Lett.*, 2012, **12**, 6353–6357.

16 G. Zhang, Y. Fu, Z. Xie and Q. Zhang, *Sol. Energy Mater. Sol. Cells*, 2011, **95**, 1168–1173.

